

The Third GABLS Intercomparison Case for Evaluation Studies of Boundary-Layer Models. Part A: Case Selection and Set-Up

Fred C. Bosveld · Peter Baas · Erik van Meijgaard ·
Evert I. F. de Bruijn · Gert-Jan Steeneveld ·
Albert A. M. Holtslag

Received: 29 August 2012 / Accepted: 13 February 2014
© Springer Science+Business Media Dordrecht 2014

Abstract We describe a novel methodology on the selection and composition of a single-case observational dataset from the comprehensive measurement program at the Cabauw observatory field site located in the Netherlands. The case can be regarded as the basis of the third case study conducted within the framework of the GEWEX (Global Energy and Water Exchange) Atmospheric Boundary-Layer Study (GABLS) and is meant to be used for the evaluation of single-column models. The ideal case is supposed to cover a period of at least 24 h with clear skies, moderate near-surface winds and a stable stratification during nighttime. From the multi-year data archive with Cabauw observations data for 1–2 July 2006 were found to best match the requirements, and were consequently selected for analysis. The dates contains a 24-h period with a nearly constant geostrophic wind of $\approx 7 \text{ m s}^{-1}$, and a considerable wind shear in the vertical. It is also characterized by a pronounced low-level jet related to an inertial oscillation that developed around sunset when the atmosphere had decoupled from the surface. Detailed initial conditions, surface conditions and dynamical forcings are derived on the basis of local observations and the outcome of a conceptual and a three-dimensional atmospheric model. It appears that a very precise prescription of the forcings is a prerequisite to enable a meaningful evaluation of models against observational data.

Keywords CESAR database · Diurnal cycle · Dynamic tendencies · GABLS · Low-level jet · Model forcing data · Single-column models · Stable boundary layer

1 Introduction

The adequate representation of the stable atmospheric boundary layer (SBL) in numerical atmospheric models is crucial for weather forecasting, climate research and chemical

F. C. Bosveld (✉) · P. Baas · E. van Meijgaard · E. I. F. de Bruijn
Royal Netherlands Meteorological Institute, De Bilt, The Netherlands
e-mail: fred.bosveld@knmi.nl

G.-J. Steeneveld · A. A. M. Holtslag
Wageningen University, Wageningen, The Netherlands

transport modelling as the atmospheric boundary layer (ABL) directly influences the conditions under which most human activities take place. The current state of affairs is that the SBL over land is only represented with a limited amount of detail in present-day large-scale atmospheric models (e.g. [Beljaars and Viterbo 1998](#); [Edwards et al. 2006](#); [Walsh et al. 2008](#); [Jung et al. 2010](#)). At the same time, the SBL has a significant impact on modelled atmospheric circulation ([King et al. 2001, 2007](#)). An inadequate representation of the SBL limits the ability to predict surface temperature ([Prabha et al. 2011](#)), the wind field ([Storm et al. 2009](#)), fog ([Velde et al. 2010](#)), dew and air pollution concentrations ([Salmond and McKendry 2005](#); [Wong and Stutz 2010](#)). The inverse modelling of greenhouse gas sources and sinks from tall tower observations (e.g., [Lauvaux et al. 2009](#); [Tolk et al. 2009](#); [Bergamaschi et al. 2010](#)) depends crucially on the representation of the SBL. In the long history of so-called case studies emphasis has been mainly on the convective boundary layer (e.g., [Lenderink et al. 2004](#); [Siebesma et al. 2004](#)). So far, limited attention has been given to case studies of the SBL over land. An essential step in improving the representation of the SBL in atmospheric models is to confront a suite of state-of-the-art models with observations of realistic situations. In general, however, the specification of forcing conditions needs to be more accurate for model *evaluation* studies than for model *intercomparison* studies (e.g. [Cuxart et al. 2006](#)). Methodologies and guidelines to achieve the required specification for model evaluation studies are presented below.

A typical single-column model (SCM) case involves the specification of initial profiles at the start of the case period, profiles of atmospheric forcings over time, boundary conditions over time at the top and bottom of the modelling domain, and parameters describing the surface characteristics. Depending on the purpose of the study these specifications can be either simple or more complex. Increased complexity can be introduced along three lines: (1) Focus on one process or take into account more processes and their interactions; (2) Perform only a model intercomparison or extend this with an evaluation against observations; (3) Evaluate against observations of state variables or also include flux observations. In practice, however, a specific case study can only be carried out when an observational site exists that matches the climate regime, or, e.g., the vegetation and soil type specified in the case. Moreover, a lack of comprehensiveness in observed parameters or data availability may pose further limitations to the method.

The Global Energy and Water Exchange (GEWEX) Atmospheric Boundary-Layer Study (GABLS) was initiated in 2001 with the goal of improving the representation of the boundary layer in regional and global models, based on a proper understanding of the relevant physics ([Holtslag 2003, 2006](#); [Holtslag et al. 2013](#)). To this end, two intercomparison studies have been performed so far, mainly focussing on the SBL. The first study covered an academic case with moderate geostrophic forcing and prescribed surface temperature. A parallel intercomparison of large-eddy simulation (LES) models served as a reference in assessing the performance of the participating SCMs. The main conclusion was that operational models utilize higher mixing efficiencies than research models, which led them to underestimate the development of the surface inversion and to overestimate the surface friction velocity ([Cuxart et al. 2006](#); [Beare et al. 2006](#)). This results in too large a cross-isobaric mass flux that has important repercussions for the representation of the larger-scale flow, as was pointed out by [Svensson and Holtslag \(2009\)](#).

The second GABLS case aimed at assessing the ability of operational and research models to represent the diurnal cycle of the ABL. This case was based on observations from the field campaign CASES-99 ([Poulos and Coauthors 2002](#)), [Steenefeld et al. \(2006\)](#) already exploited the ability to represent this dataset by an SCM. For this GABLS case the models were run with a prescribed surface temperature in order to focus on the comparison of the

turbulence schemes. [Svensson et al. \(2011\)](#) showed that even in such a set-up atmospheric temperatures varied substantially among models due to differences in interaction between stability and fluxes. Although the second GABLS case was derived from detailed observations, the prescribed forcings to the atmospheric column lacked the accuracy needed for a quantitative comparison between models and observations. Furthermore, prescribing the surface temperature has a trade-off: it inhibits the modelled SBL from interacting with the surface, a process that is recognized as being crucial for the development of the SBL ([Wiel et al. 2003](#); [Holtslag et al. 2007](#)). Here we instigate a follow-up case that overcomes many of the shortcomings mentioned above.

A third GABLS intercomparison case (GABLS3) for SCMs and LES has been set-up on the basis of observations from the Cabauw measurement site in the Netherlands. The focus of the current case is on the representation of decoupling around sunset, the subsequent development of the low-level jet (LLJ) and the morning transition. Due to the flat surface conditions, Cabauw is especially suited to study the LLJ that arises from inertial oscillations ([Baas et al. 2009](#)). Recent research shows that model results in stable conditions are strongly influenced by the description of the lower boundary condition ([Holtslag et al. 2007](#); [Basu et al. 2008](#)). In the GABLS3 case the models are fully interactive with their soil-vegetation scheme, and as such we extend earlier GABLS studies by adding this complexity. No upper boundary condition is prescribed since the models operate with the complete atmospheric column. Special attention is given to an accurate prescription of large-scale atmospheric forcing, which should enable a direct evaluation of the SCM results against observational data.

We describe the GABLS3 SCM case set-up and provide background information on the observations and three-dimensional (3D) atmospheric model runs used to specify the case. An accompanying paper ([Bosveld et al. 2014](#)) presents the results of the SCM intercomparison and evaluation. [Basu et al. \(2012\)](#) compare the results obtained from LES models that are run for an adapted version of the current case.

2 Observations

2.1 CESAR Measurement Program

The Cabauw Experimental Site for Atmospheric Research (CESAR) is located in the western part of The Netherlands (51.971°N, 4.927°E); the distance to the North Sea is 50 km in a west-north-west direction. Variations in surface elevation are very small (<1 m), while the River Lek flows 1 km south-east of the site. The environment is dominated by grassland, fields, scattered villages and tree lines, with the soil consisting of a 0.7-m thick clay layer on top of a thick peat layer. The ground water table is managed by a dense network of ditches, and only rarely does soil drying lead to transpiration reduction of the grassland. The terrain around the 200-m main tower is free from obstacles up to a few hundred m in all directions. More details and site characteristics can be found in [Ulden and Wieringa \(1996\)](#), while [Beljaars and Bosveld \(1997\)](#) describe the observational datasets for the period 1986–1996.

After modernisation of the site, the observations resumed in 2,000 resulting to date in a dataset covering over 20 years. In 2002 the CESAR consortium was founded that consists of eight institutes, and resulting in a comprehensive set of observations of the atmospheric column and the underlying surface ([Russchenberg et al. 2005](#)). Here we focus on the observations related to the ABL and its interaction with the surface. The measurement program includes vertical profiles of wind speed, wind direction, temperature and humidity along the tower (at heights $z = 10, 20, 40, 80, 140$ and 200 m), as well as all components of the

surface radiation and energy budgets. Soil thermal conditions and soil water conditions are continuously monitored. Moreover, the tower is equipped with turbulence instruments at four heights, which measure profiles of the turbulent fluxes of momentum, heat, moisture and CO₂. These data are archived as 10-min mean values. A wind-profiler/RASS system measures wind speed, wind direction and virtual temperature at levels exceeding the tower top and these observations are archived as 30-min mean values. From 2001 onward, most of these data sources are continuously available, with tower flux observations becoming gradually available since 2003.

Until 2012, twice a day (0000 and 1200 UTC), radiosoundings are available from weather station De Bilt (station 06260), which is located 25 km to the north-east of Cabauw. Especially for the lowest part of the sounding this horizontal distance may give rise to differences with the actual profile at Cabauw, depending on the wind direction in relation to the upwind surface conditions.

2.2 Surface Geostrophic Wind

The geostrophic wind is an important parameter affecting the structure of the SBL. For Cabauw it can be derived from pressure observations obtained with the Dutch national meteorological network, and in the current network pressure observations are stored with a frequency of 10 min (last 1-min average) from December 2002 onward. A longer time series exists of hourly values (last reading in the hour). Over time, a number of sea locations has been installed, which are useful for the determination of geostrophic wind in the western part of The Netherlands. The pressure readings are reduced to mean sea level according to prescriptions of the World Meteorological Organization, taking into account the effects of temperature and humidity on the weight of the air column. Because the surface elevation, relative to the mean sea level, of the stations involved is very small this reduction to one horizontal plane can be done very accurately. The accuracy in estimated sea surface pressure is 0.1 hPa.

The geostrophic wind field over the Netherlands has in the past been derived by means of a principle component analysis of the observed pressure field as obtained from all available land-surface pressure observations (e.g. [Nieuwstadt and Driedonks 1979](#)). This method is very efficient for the characterization of the horizontal field. Geostrophic winds for a specific location can be adequately derived by fitting the pressure observations to a polynomial expansion with the x - and y -directional coordinates as arguments. Estimating the geostrophic wind for one location is a trade-off between high resolution in time, which results from using only nearby stations, and high accuracy, which increases by using more and more distant stations. Moreover, as stations at greater distance are used, the more need there is to include higher-order terms in the expansion, increasing the number of parameters to fit.

Various estimates of the zonal and meridional geostrophic wind components (U_G and V_G , respectively) have been derived by varying the threshold distance to Cabauw below which a pressure station is incorporated in the calculation. Also linear and quadratic approximations to the pressure field in terms of the horizontal coordinates have been examined. A good result was found by using a quadratic regression field composed of pressure observations at 20 stations located within a radius of 150 km. The standard error amounts to 0.31 m s^{-1} and 0.33 m s^{-1} for U_G and V_G respectively, with negligible correlation between the errors in the two components. This is the version that we used for the GABLS3 case.

2.3 Characterization of the Large-Scale Forcings with an Atmospheric Model

To obtain realistic results from an SCM run, the model needs to incorporate realistic vertical profiles of the geostrophic forcing (pressure gradient) and of the dynamical tendencies of wind, temperature and humidity induced by the synoptic-scale weather conditions. We call these the large-scale forcings. In general, information on the large-scale forcings at higher levels in the atmosphere is not available from direct observations. To estimate the size of the required forcings we resorted to information provided by the KNMI regional climate model RACMO (van Meijgaard et al. 2008), which employs the dynamics kernel of the High Resolution Limited Area Model (HIRLAM) and the physics package of the European Centre for Medium-Range Weather Forecast (ECMWF) model. For this purpose, a short-term integration with the RACMO model at 18-km horizontal resolution and 40 levels in the vertical was carried out in hindcast mode utilizing operational analyses from ECMWF for initialization and forcing at the lateral boundaries of the domain. The run was initialized at 0000 UTC, 1 July 2006 and integrated for 36 h, from which the last 24 h cover the case period. No data assimilation is applied. Model fields from the grid point closest to Cabauw and the eight surrounding grid points were stored for all model timesteps. Based on this information the vertical structure of the geostrophic forcings and dynamical tendencies and their evolution in time are calculated. Analysis of sensitivity runs performed at increasing resolution led to the conclusion that the signature of most of the model parameters is reasonably independent of the resolution with the exception of the vertical dynamical tendency. For some specific applications in this study a SCM version of RACMO is used (RACMO-SCM).

3 Case Selection and Description

3.1 Selection

Six years of data (2001–2006) were examined to select a suitable case for GABLS3. To avoid conditions with undesirable complexity, the ideal case has to satisfy at least three criteria: a stationary synoptic situation, clear skies and the absence of fog. Additionally, a significant surface inversion must develop after sunset with a distinct LLJ directly aloft. For the development of a substantial LLJ a moderate geostrophic forcing of about 7 m s^{-1} is favourable (Baas 2009). A first selection was made by searching the archive for cases with a geostrophic forcing between 5 to 10 m s^{-1} , with less than 3 m s^{-1} variation during the night, and a net longwave cooling $>30 \text{ W m}^{-2}$ at night as an indicator of cloud-free conditions. From all six years examined, only 28 nights (1.3%) passed these criteria. For these cases three additional criteria were applied: the synoptic situations had to be relatively stationary; the water vapour deficits had to be large enough to avoid dew formation and malfunctioning of instruments; the advective tendencies (estimated by using trends in the nighttime 200-m temperature, see Sect. 5.2 below) had to be small. After these selections nine potential cases remained.

The selection of a small subset of typical cases can be used to distinguish between general characteristics and case-specific features. For example, Fig. 1 shows time series of the 200-m wind speed for the nine selected nights. All cases show the general characteristics of an inertial oscillation. However, in more detail, every case evolves differently due to subtle differences in, for example, the geostrophic forcing or the large-scale advection of momentum (Baas et al. 2010). Through inspection of the tower observations, surface analysis charts, and data availability the most suitable case for GABLS3 was chosen: the night of 1–2 July 2006.

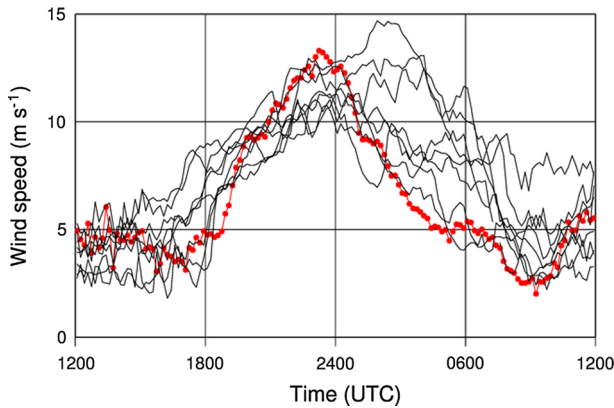


Fig. 1 Diurnal cycle of the 200-m wind speed for nine clear nights with comparable geostrophic wind speed ($\approx 7 \text{ m s}^{-1}$). The red-dotted line is the finally selected case period 1–2 July 2006

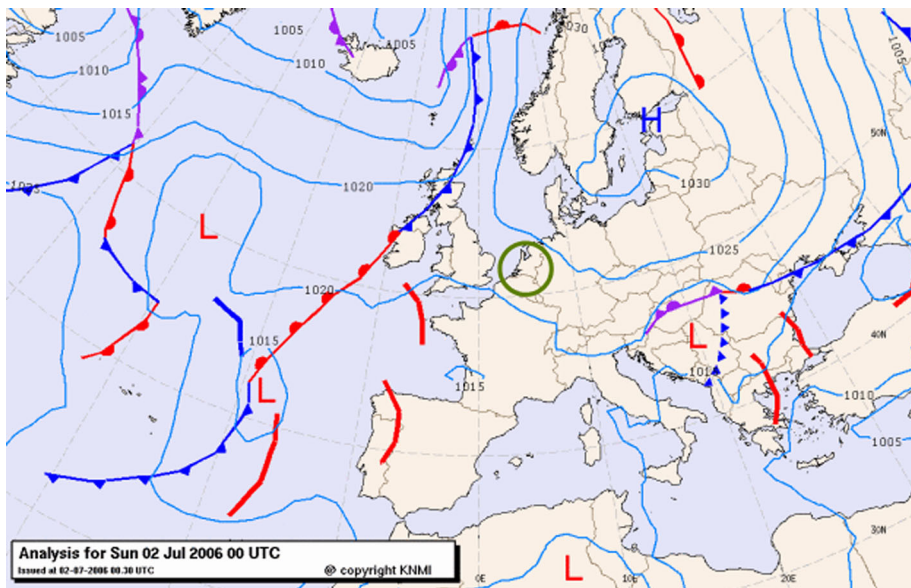


Fig. 2 Surface pressure analysis showing the synoptic situation for the GABLS3 case at midnight (2 July 2006 0000 UTC). The centre of the green circle represents Cabauw, The Netherlands

3.2 Characterization of the GABLS3 Case

The GABLS3 case (1–2 July 2006) is characterized by easterly flow near the surface around a high pressure area above the Baltic Sea (Fig. 2). The large-scale synoptic situation is rather stationary over the period of interest. The geostrophic wind decreases with increasing height, corresponding with warmer air to the south or, equivalently, a southward tilt of the axis of the high-pressure system, veering a little in the course of the night.

For the current episode, both satellite observations and radiation measurements indicate cloud-free conditions. In Fig. 3 radiosoundings at three times during the simulation period are

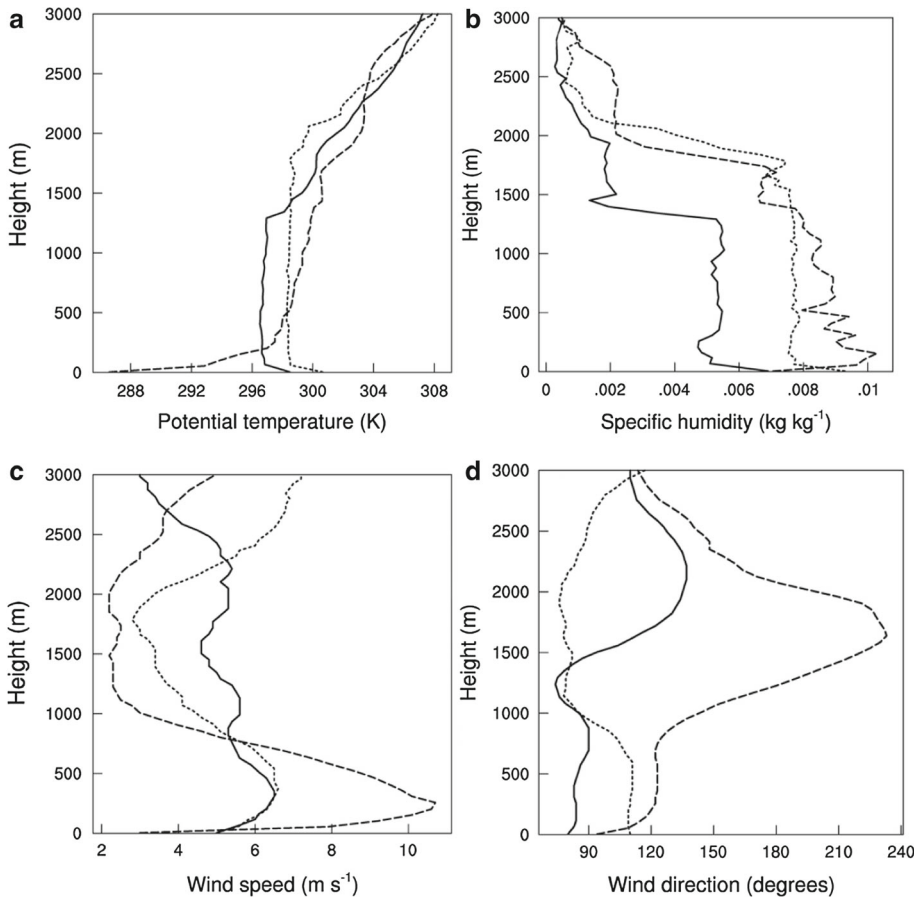


Fig. 3 De Bilt radiosounding at noon (*solid*), midnight (*dashed*) and the next noon (*dotted*) for **a** potential temperature, **b** specific humidity, **c** wind speed and **d** wind direction

shown, i.e. at noon of the first day, at midnight and at noon of the second day. A significant decrease of wind speed with height is observed (panel C), and a well-mixed convective boundary layer is observed in the two noon soundings (panels A and B). The sounding at 1 July 2006 1200 UTC indicates the presence of a relatively shallow, cool and dry boundary layer of about 1,300 m depth. This is confirmed in Fig. 4a–d where time series of the basic meteorological parameters along the 200-m tower are shown; Fig. 4d shows relatively low dewpoint temperatures at the start of the case period, compared to the later stage of the case. Wind-profiler observations (not shown here) indicate that the ABL height increases rapidly after noon, suggesting that a column of dry air passes the site at the start of the simulation period (1200 UTC), but is quickly replaced by an air mass with more humid air and a deeper boundary layer of depth around 2,000 m.

A few hours before sunset, the air temperature at 2 m reaches its maximum value of 27°C, but already before sunset, rapid cooling occurs near the surface. The rapid decline of turbulence in the former mixed layer initiates a clear inertial oscillation in the wind field. By the end of the night the potential temperature difference between 2 and 200 m in the tower amounts to 9 K. Wind direction at 10 m varies between 80 and 120°. From 0000–0300 UTC

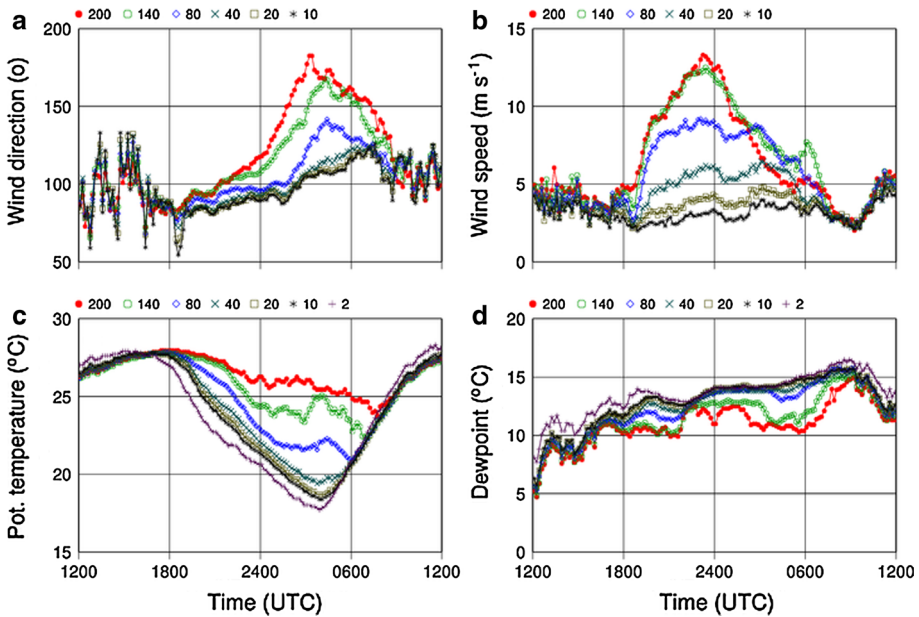


Fig. 4 Observed **a** wind direction, **b** wind speed, **c** potential temperature and **d** dewpoint temperature at 6 (7) levels in the Cabauw 200-m tower for the case period. Here potential temperature is relative to the surface level

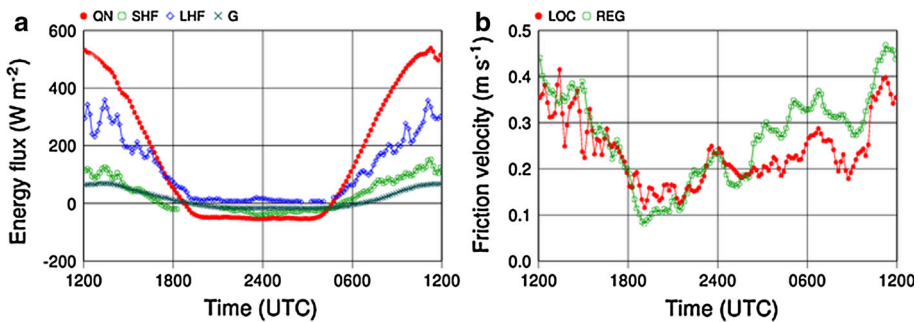


Fig. 5 **a** Observed components of the surface energy budget, where QN is net radiation, SHF is sensible heat flux, LHF is latent heat flux and G is soil heat flux. **b** Friction velocity where LOC is the local friction velocity and REG is the regional friction velocity

a small synoptic disturbance is advected over the site, resulting in variations in temperature, humidity and wind. This is best seen in the dewpoint temperature at 200-m height (Fig. 4d) and is further investigated in Sect. 5.

Figure 5a shows the components of the surface energy budget with large values for the latent heat flux during daytime that is typical for Cabauw; Fig. 5b shows the friction velocity inferred at both the local and the regional scale. The friction velocity at the local scale is derived from sonic anemometer observations by means of the eddy-correlation technique, and is representative of the smooth grass land at the site with a typical horizontal scale of 100 m. The friction velocity at the regional scale is derived from the 10-m wind speed, the potential temperature vertical difference in the lowest 10 m and a regional-scale roughness length.

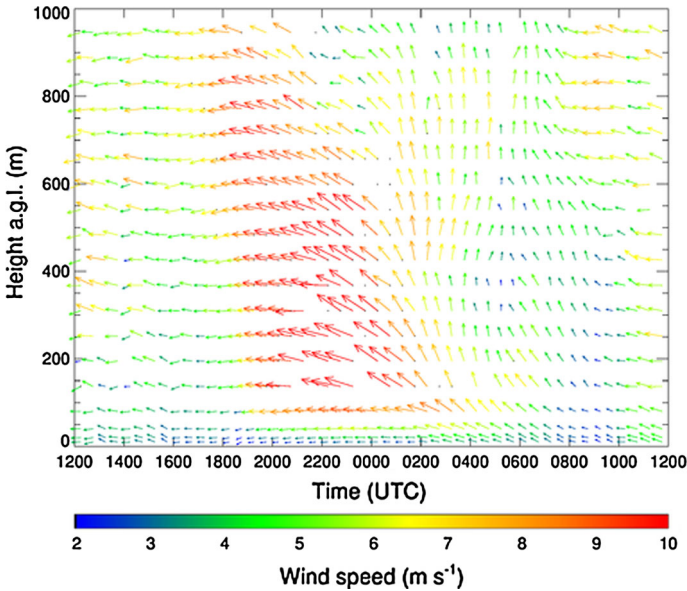


Fig. 6 Observed wind vectors between 1 July 2006 1200 UTC and 2 July 2006 1200 UTC. Data are a composite of wind profiler and tower observations

It is representative of a scale of 1 km including the effect of tree rows and other obstacles in the upwind direction and has therefore a higher value than the local friction velocity. Values are comparable until 0200 UTC, after which the regional-scale friction velocity is larger than the local-scale friction velocity. Finally, Fig. 6 shows the horizontal wind vectors as measured by the wind profiler. The LLJ reaches its maximum of 12 m s^{-1} shortly before midnight, with the height of the wind maximum situated around 200 m above ground level, and with the inertial oscillation visible up to $\approx 1,000 \text{ m}$.

4 Case Set-Up

The case comprises 24 h commencing at 1200 UTC (1220 local mean solar time) on 1 July 2006 and ending at 1200 UTC the next day. The Appendix presents the complete case set-up, and describes the characterization of the land-surface properties required for the modelling of land-atmosphere interaction, the initial conditions in the soil and the atmosphere, the geostrophic forcing and finally the dynamical tendencies as a function of height and time.

4.1 Surface Characteristics

The required surface albedo is determined from local radiation measurements at Cabauw, and was found to vary slightly with solar elevation and with vegetation conditions. A representative value of 0.23 was obtained, and is consequently prescribed in the model intercomparison study. The surface emissivity is not measured at the site, and therefore we prescribe a value of 0.99, since a fully covered vegetation layer, as present at the Cabauw site, will have an emissivity close to 1.0. Finally, the leaf area index $LAI = 2$.

Locally at the grassland around Cabauw a roughness length of 0.03 m is observed. The SBL generally develops over a relatively large upwind terrain and, therefore, we use the regional-

scale roughness length for momentum (z_{0M}) based on observations of the standard deviation of the horizontal wind (Beljaars 1987; Beljaars and Bosveld 1997). For summertime and for the wind directions of interest, i.e. between 60 and 120 degrees, $z_{0M} = 0.15$ m. Verkaik and Holtslag (2007) showed that this value closely agrees with observations of the stress at higher levels in the 200-m tower. They also showed that at intermediate levels (e.g. 20 m) the drag is higher than the regional-scale value due to the presence of the village of Lopik. Both studies concentrated on near-neutral conditions, and the applicability of their findings to stable flows was not investigated. The interaction of the stable flow, which in general resists upward motion, with tree rows and other obstacles, may lead to a different flow regime that requires characterization by a different effective roughness length.

The physical mechanism through which obstacles extract momentum from the flow (pressure drag) is absent for heat transport; therefore, a local-scale estimate of the roughness length for heat, z_{0H} , seems to be appropriate. The roughness length for heat is estimated from the observed surface radiation temperature of the local grassland, the air temperature at 1.5-m height, and the sensible heat flux. A typical value of $z_{0H} = 1.5$ mm is found, which is 5% of the local-scale roughness length for momentum. This is slightly less than the typical ratio of $z_{0H}/z_{0M} = 0.1$ (Brutsaert 1982).

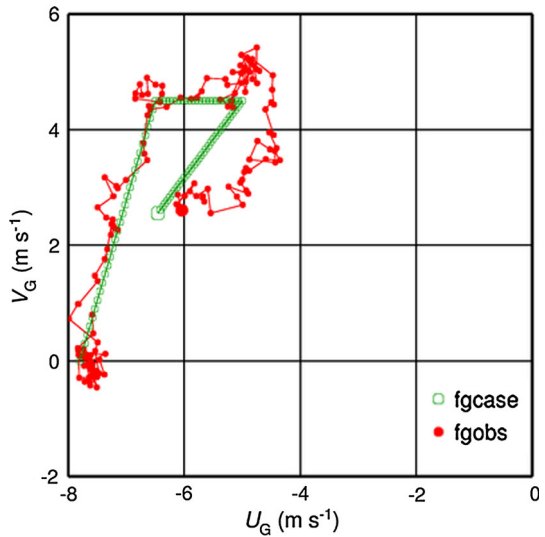
Surface evaporation from the grassland plays a dominant role in the daytime surface energy balance at Cabauw. The modelled evaporation depends strongly on the prescribed soil moisture content, and on the details of the land-surface scheme. As only a fixed amount of energy is available for evaporation and heating of the ABL, this implies that the soil moisture influences the evolution of the convective boundary layer (Heerwaarden and Vila-Guerau de Arellano 2009). To ensure that the magnitudes of the modelled turbulent fluxes are consistent with the observations, the soil moisture content in each model should be chosen such that the Bowen ratio equals 0.33 at initialization. This corresponds to the value observed at Cabauw around 1200 UTC.

For each model a soil type needs to be chosen that approaches as close as possible the soil type profile at Cabauw. At the site, the following layers can be distinguished in the soil: layer 0–0.03 m, turf zone; layer 0.03–0.18 m, 35–50% clay (particles $\leq 2 \mu\text{m}$) and 8–12% organic matter with high root density; layer 0.18–0.60 m, 45–55% clay and 1–3% organic matter with low root density; layer 0.60–0.75 m, a mixture of clay and peat; layer 0.75–7 m, peat. The dry density of the clay typically amounts to $1,100 \text{ kg m}^{-3}$, and the water content amounts to 60% (by soil volume) at saturation and 40% at the wilting point.

4.2 Initial Conditions

The initial value of surface pressure is 1,024.4 hPa. The initial profiles of temperature, wind and humidity are derived from radiosoundings and tower observations. As discussed in Sect. 3, a relatively dry air mass with a shallow ABL passed Cabauw at the start of the simulation period at 1200 UTC. Using this sounding to initialize the model would result in a too dry boundary layer, a too low ABL height (1,300 m) and too low values for longwave incoming radiation (not shown). Since the first few hours of the simulation are not the focus of our evaluation, we omitted this feature from the simulation by excluding the corresponding advective tendencies from the set-up. Instead, to initialize the model, we used the profiles of the deeper and more humid ABL (2,000 m) as observed around 1500 UTC. The profiles are given as piecewise linear functions that, if required, can be interpolated to the specific model grid. Finally, the initial soil temperature profile is taken from local observations around 1200 UTC, and is also given as a piecewise linear function.

Fig. 7 Time trace in the horizontal plane (zonal and meridional component respectively) of surface geostrophic wind from observations (fgobs) and as prescribed piecewise linearly for the case (fgcase) for the 24-h simulation period. U_G is the zonal and V_G is the meridional component; the timestep is 10 min. *Large symbols* represent the end of the period



4.3 Geostrophic Forcing

The surface geostrophic forcing at Cabauw is estimated from surface pressure observations (Sect. 2.2), and a piecewise linear approximation is used for the case prescription. Figure 7 shows the observed and prescribed course of the surface geostrophic wind. Note that several periods with approximately constant geostrophic wind-speed components can be distinguished, seen as clustering points in Fig. 7, with rapid changes between the clusters. At 1200 UTC $U_G = -7.5 \text{ m s}^{-1}$ and $V_G = 0$. At 2300 UTC the geostrophic wind has turned such that $(U_G, V_G) = (-6.5, 4.5) \text{ m s}^{-1}$, while V_G remains constant at that value until 0600 UTC the next morning, and afterwards rapidly decreases to 2.5 m s^{-1} at noon. In that time frame, U_G develops from -6.5 to -5 m s^{-1} between 2300 UTC and 0300 UTC, and the next morning U_G increases slightly between 0600 UTC and 1200 UTC to -6.5 m s^{-1} . We choose to represent the three well-defined clusters and the end of the period as fixed points in the piecewise linear approximation. To estimate the vertical variation of the geostrophic wind, we resorted to the 3D RACMO simulation of the case. Figure 8 shows that the geostrophic forcing decreases with height. Based on this model result a constant forcing of $(U_G, V_G) = (-2, 2) \text{ m s}^{-1}$ is applied at altitudes above 2 km. Between 2 km and the surface a linear interpolation is performed for the sake of simplicity.

5 Derivation and Impacts of Dynamical Tendencies

The accuracy of prescribed advective tendencies is important in the simulation of atmospheric profiles using the SCM (e.g. Teixeira and Miranda 2001; Bergot et al. 2007). Baas et al. (2010) and Neggers et al. (2012) use advection terms derived directly from the analysis of 3D numerical weather prediction models. Advective tendencies in these models likely depend on the physical parametrization of the model. Although they represent genuine physical processes, it is not a priori clear to what extent they correspond to the actual advective tendencies in the real atmosphere.

Over the years, improvements in the parametrization of atmospheric processes, increases in model resolution, and the assimilation of more detailed observations have led to a better

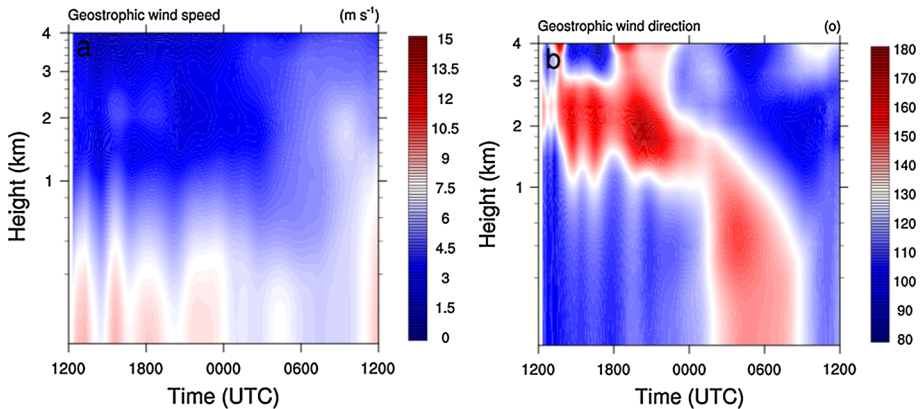


Fig. 8 Time-height diagrams of geostrophic wind speed (**a**) and geostrophic wind direction (**b**) for 1 July 2006 1200 UTC to 2 July 2006 1200 UTC, as simulated by the RACMO-3D model

representation of the state of the atmosphere and presumably also to a better description of advective tendencies. Bosveld et al. (2004) compared horizontal advective tendencies from the 3D RACMO model with tendencies derived from flux-divergence observations made at the Cabauw 200-m tower. With a grid cell size of 25 km a reasonable agreement during daytime convective conditions was found for two selected days, one with advection and one without advection. This grid cell size assumed that at least one land grid cell was situated between the Cabauw grid cell and the North Sea, preventing the model horizontal diffusion dominating the contributions from advection. Baas et al. (2010) showed that the correlation between the dynamical tendencies generated by a 3D numerical weather prediction model on the one hand, and the observed development of the nocturnal jet on the other, increased significantly when considering a composite of nine nights instead of individual nights. This suggests that the model is not capable of providing real-world mesoscale features in a deterministic way, whereas mesoscale variability can have a significant impact on the dynamics of the atmospheric column.

Dynamical tendencies can in principle be derived from observations of the vertical divergence of the turbulent fluxes along a single tower (Casso-Torralba and Vilà-Guerau de Arellano (2008)). However, divergences are relatively small and practical application of the method is hampered by the fact that local scale advection induced by upwind inhomogeneities in the landscape may disturb the divergence. Also, inter-comparability issues with the turbulence instruments may complicate the interpretation of the measurements. A dense network of synoptic observations contains, in principle, also information on advection. In practice, especially during nighttime, local differences in near-surface temperature, humidity and wind speed, induced by small-scale land-surface characteristics and obstacles will hamper the applicability. During nighttime, when the interaction with the surface is small, changes in observed wind, temperature and humidity at levels sufficiently far away from the surface may indicate contributions from dynamical processes. Here, we attempt to derive dynamical tendencies for this case by examining the results of the 3D RACMO run and the observed rate of change of observations at 200-m height at night.

5.1 Model Results

Horizontal dynamical tendencies are derived from the 3D RACMO model by applying the advection operator to the variables of interest, i.e. temperature, humidity and momentum.

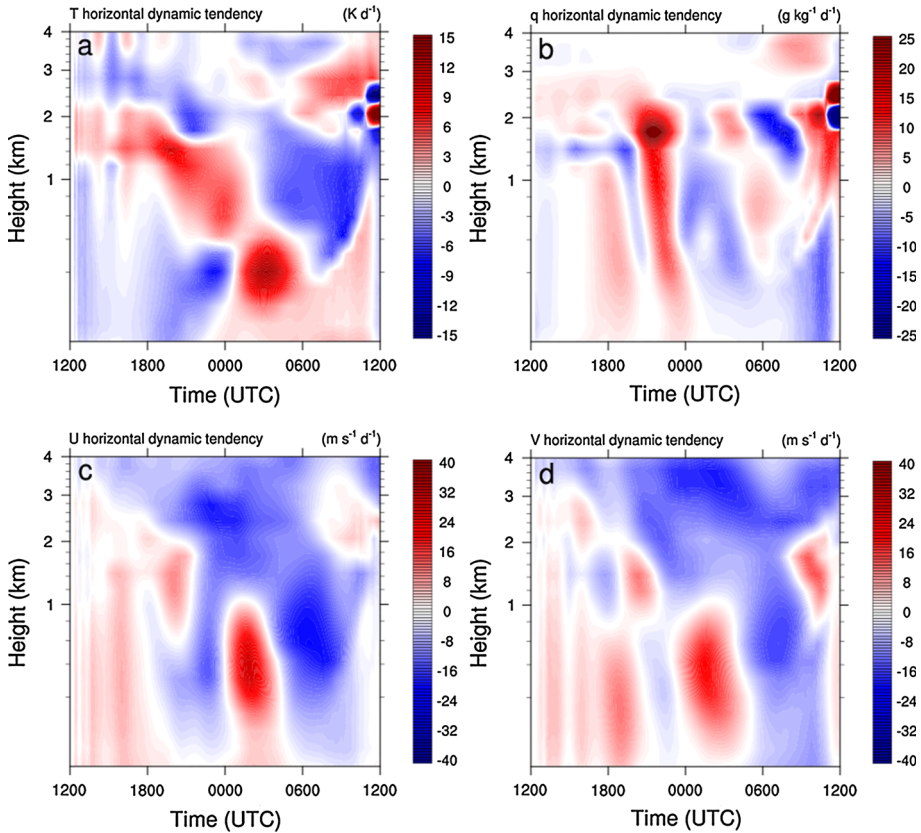


Fig. 9 Time-height diagrams for 1 July 2006 1200 UTC to 2 July 2006 1200 UTC of horizontal dynamical tendencies of temperature (a), humidity (b), zonal wind (c) and meridional wind (d) as simulated with the RACMO-3D model

We also estimated the tendencies directly from the semi-Lagrangian calculation of the dynamic equations in RACMO. Differences between both methods appeared to be small.

The passage of a small-scale synoptic disturbance during the simulated night is well-illustrated in Fig. 8 where the simulated geostrophic wind speed is shown to be nearly constant in time. Geostrophic wind direction shows a marked veering shortly after midnight. Figure 9 shows horizontal dynamical tendencies of temperature, humidity and momentum. Cool air advection in the lowest 300 m up to 10 K day^{-1} before midnight is followed by a distinct episode of warm air advection up to 10 K day^{-1} that reaches the surface after midnight. In the lowest part of the atmosphere moisture advection of $5\text{--}10 \text{ g kg}^{-1} \text{ day}^{-1}$ takes place during the first half of the night followed by drying of up to $5 \text{ g kg}^{-1} \text{ day}^{-1}$ after midnight. The horizontal dynamical tendencies of the zonal and meridional wind components show a negative zonal tendency in the lowest 1,000 m before midnight and a significant positive tendency after midnight in both components, ranging from -12 to $+20 \text{ m s}^{-1} \text{ day}^{-1}$. In the next section, a combination of model-based horizontal dynamical tendencies and local observations is used to specify the final case prescription of horizontal dynamical tendencies.

As mentioned in Sect. 2.3, modelled vertical dynamical tendencies are resolution dependent. Since we have no other source of information available, we continue to resort to the

model results. For a range of different model resolutions, a vertical motion of 0.12 Pa s^{-1} (subsidence) at 1,500 m is found until 1700 UTC of the first day. From that time on the signal becomes variable and dependent on resolution. Given this uncertainty we set vertical motion to zero after 1700 UTC, and in the case prescription, the vertical motion below 1,500 m is linearly interpolated to zero at the ground.

5.2 Local Observations

Observed tendencies at one location are typically the sum of physical and dynamical tendencies. Deriving dynamical tendencies from local observations is only possible when detailed information on the physical tendencies is available, which is in general not the case. However, during stable conditions the air layer above the turbulent SBL often becomes decoupled from the surface, inducing relatively small physical tendencies. Here we use this feature to qualitatively assess whether the advective tendencies derived from the models actually resemble the advective tendencies directly inferred from observations at Cabauw. To achieve this, we employ observations at the 200-m level, which was located at the top of the SBL during this specific night.

We apply the prognostic equations for momentum, temperature and humidity at a height of 200 m, while ignoring the physical processes but retaining the influence of geostrophic wind and the Coriolis acceleration on the momentum budget,

$$\frac{\partial S}{\partial t} = -U \frac{\partial S}{\partial x} - V \frac{\partial S}{\partial y}, \quad (1a)$$

$$\frac{\partial U}{\partial t} = -U \frac{\partial U}{\partial x} - V \frac{\partial U}{\partial y} + f(V - V_G), \quad (1b)$$

$$\frac{\partial V}{\partial t} = -U \frac{\partial V}{\partial x} - V \frac{\partial V}{\partial y} - f(U - U_G), \quad (1c)$$

where S is any of the scalar parameters, temperature or humidity, U and V are the zonal and meridional wind components and f is the Coriolis parameter. We call these the simplified prognostic equations (SPE). The 200-m wind, temperature and specific humidity are initialized by the observed values before sunset (around the moment of decoupling), and then the SPEs are integrated forward in time, while forced by the observed surface geostrophic wind as derived in Sect. 2.2. We applied the SPEs with various prescriptions of the horizontal dynamical tendencies, to find an optimal prescription that matches the observed nighttime 200-m temperature, humidity and wind components best (see Appendix).

Figure 10 shows the evolution of temperature and specific humidity obtained by integrating the SPEs with the horizontal dynamical tendencies as prescribed for the case, and as derived from the 3D RACMO model. A significant temperature decrease due to radiative cooling is found in the observations, which is not accounted for in the SPE (Fig. 10a). A minor cooling, and after midnight, warming with an integrated amplitude of 0.5 K is observed in the run using the RACMO tendency. A comparable variation is superimposed on the cooling trend in the observations. For specific humidity (Fig. 10b) the passage of more humid air with a perturbation of 1 g kg^{-1} is observed around midnight. This is reasonably well captured by the simulation using the RACMO-3D tendency although with a smaller perturbation. For the GABLS3 case the specific humidity tendency is prescribed with a piecewise linear function, with an amplitude comparable to the observations.

The evolution of the observed wind vector at 200 m together with the observed geostrophic wind is shown in a U - V diagram in Fig. 11. Also shown are the results from the integration of the SPE forced with and without momentum tendencies derived from the 3D RACMO

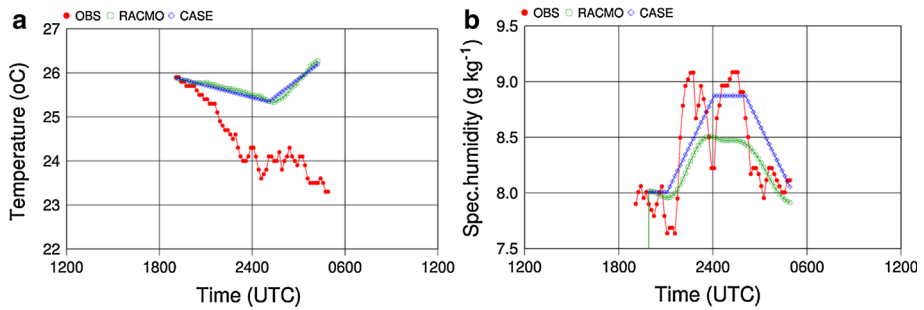


Fig. 10 Evolution at 200 m as observed (OBS) and modelled by the SPE model using RACMO-3D and CASE advection for **a** temperature and **b** specific humidity

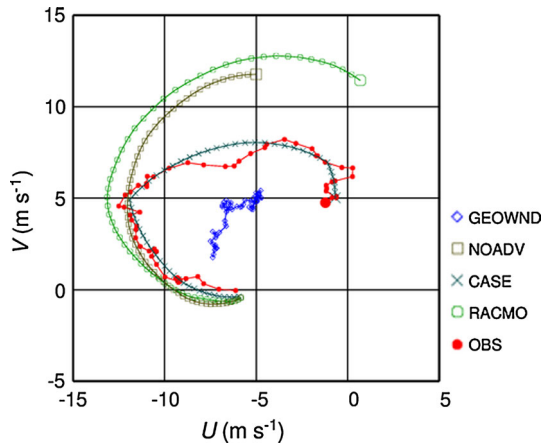


Fig. 11 Evolution at 200 m as observed (OBS) and modelled by the SPE model using RACMO-3D and CASE advection for horizontal wind; U is the zonal and V is the meridional component. Additionally, the geostrophic wind evolution (GEOWND) and the SPE model results when neglecting the advection (NOADV) are shown. Start of time series is at 1830 UTC (moment of decoupling); the end of the time series is 11 h later (indicated by *large symbols*); The timestep is 10 min. In all simulations the observed geostrophic wind is used

model. The effect of momentum advection is quite complex due to the interaction with the Coriolis force and the changing geostrophic wind. We find that the SPE without advection and with tendencies obtained from the 3D RACMO model do not represent the observed 200-m wind accurately. The dynamical tendencies of momentum for the GABLS3 case have been estimated by adjusting these tendencies until a reasonable agreement between observed 200-m wind and the SPE simulated wind was obtained. This integration is also shown in Fig. 11.

5.3 Impact of Dynamical Tendencies on SCM Results

As shown in the previous section, temperature and humidity are influenced by their respective dynamical tendencies in a straightforward way. For wind the influence of the dynamical tendency is more complex due the interplay with the geostrophic wind and the inertial oscillation. Figure 12 shows time series of the 200-m wind as observed and as simulated with the RACMO-SCM. The simulations were performed first with the full prescription of the GABLS3 case, and then once by neglecting the dynamical tendencies for the wind

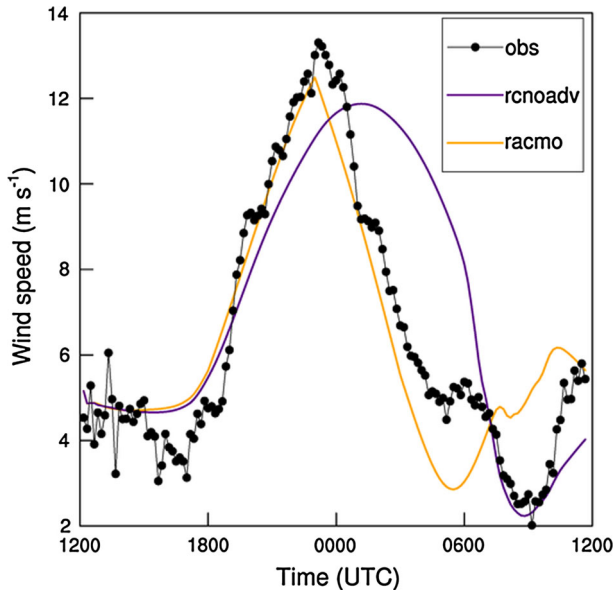


Fig. 12 Simulation of the wind speed at 200-m height with RACMO-SCM for the GABLS3 case with (racmo) and without (rcnoadv) dynamical tendency. Also shown are the observations (*black dots*)

components. Evidently, the presence of dynamical forcings in the SCM simulation has a significant influence on the evolution of the 200-m wind at night. The developing LLJ is quite abruptly ended by the advection of momentum, whereas without advection the LLJ continues much longer into the following day. To conclude, without an accurate prescription of dynamical tendencies, the SCMs would deviate too far from reality, making a comparison with observations meaningless.

6 Discussion and Conclusions

We presented the third GABLS case for model evaluation, where a novel methodology is designed to obtain atmospheric forcings that are sufficiently accurate to allow for a direct comparison between models and observations. From an archive of six years of observations from Cabauw we were able to select nine cases that matched, to a reasonable degree, the defined criteria. This encouraging result underlines the value and importance of performing comprehensive long-term continuous measurement programs. However, none of these cases was stationary in terms of atmospheric forcings and without an accurate prescription of these forcings a direct comparison of the model simulations with observations is impossible. The observed variations in the geostrophic wind seem typical for clear-sky summertime nights at Cabauw that are dominated by easterly winds. As shown by [Delden \(1993\)](#) and [Tijm et al. \(1999\)](#) these variations are induced by the presence of the temperature contrast between the land and the neighbouring North Sea.

[Baas \(2009\)](#) analyzed the observed mesoscale disturbance that passed over Cabauw at midnight, 1–2 July 2006 in more depth using the RACMO-3D model. He found that around sunset the model generates a disturbance in the hills 150 km south-east of Cabauw, which propagates in the north-westerly direction and passes over the site at midnight. It is interesting

to note that no data assimilation is applied in the model and that the disturbance is not imported into the model domain by the ECMWF model but generated internally. In [Baas et al. \(2010\)](#) a number of comparable cases were analyzed, all were subject to various mesoscale disturbances. They concluded that on a night-by-night basis the model dynamical tendencies lack the accuracy to serve as forcing of the realistic SCM simulations. However, they also found that, when using a composite of several comparable nights, contributions from random mesoscale disturbances showed a tendency of cancelling out, which led to a much improved evaluation of the composed SCM simulation with composed observations. In the current study we show that a realistic case for an individual day can be set-up by augmenting the 3D model results with observational information from a well-instrumented site.

Initial profiles of soil temperature were taken directly from the local observations, and in reality this soil profile will be in thermodynamic equilibrium with the surface energy fluxes. The initial atmospheric profile is adapted to account for the dry air mass that was advected over the site at the initialization time, implying that the soil and atmospheric profiles are not in thermodynamic equilibrium. Even if we had taken the observed initial atmospheric profile, there will in general be no equilibrium in the models, because their description of the soil-vegetation system and of the interaction with the atmosphere will differ from reality. Transient effects occur in the first few hours of the simulation, yet we expect these adjustment effects to die out by sunset in the model simulation. Still, this initial thermal imbalance may induce longer-term deviations in the temperature and humidity in the convective boundary layer. A roughness length for momentum is prescribed that is representative of the regional scale; this is a simplification of the actual influence of tree rows and a small village that are present in the first 3 km upwind from the tower. In addition blocking of the flow and thermal effects induced by the village may, during stable conditions, affect the properties of the lowest portion of the atmosphere in a way not accounted for in model simulations.

For dynamical tendencies we relied partly on RACMO-3D model runs, but we also attempted to simulate dynamical tendencies for this case with two other regional models, HIRLAM ([Undén et al. 2002](#)) and WRF ([Skamarock and Klemp 2008](#)). Although the three models showed qualitative agreement in representing the tendencies of some of the parameters, even for these parameters significant differences in magnitude were found. The RACMO-3D model was chosen because it compared best with the observed dynamical tendencies, indicating again that the use of dynamical tendencies from 3D models to drive SCMs needs to be done with caution. For this case the use of observations to estimate the dynamical tendencies turned out to be very beneficial.

The way case studies for model validation and/or evaluation are defined will vary with the purpose of the study and the available observations. For model intercomparison one may use an idealized case since comparison with observations is not necessary; this was the route chosen for the first GABLS case. For model evaluation the case should be sufficiently realistic to allow for a direct comparison with observations. When studying a specific process in isolation the constraints set on the case will be different than for a study of the interaction between various processes. For example, studying the turbulent exchange in models without interaction with the land surface can be done by imposing a prescribed lower boundary condition. This was the approach in the second GABLS case set-up. When adding interaction with the land surface the attribution of differences among models becomes more complex. This is pursued in the current third GABLS case, where [Bosveld et al. \(2014\)](#) show that it is still possible to unravel the interactions and attribute model deficiencies to problems in the parametrization of specific processes in the models. The current case can be seen as a logical step in a sequence of increasingly realistic cases with increasing complexity.

Regarding the set-up of an SCM evaluation case study, when compared to the more traditional model intercomparison study, we conclude that:

- The set-up of a model evaluation study poses higher requirements on the specification of the forcing conditions than is needed for a model intercomparison study
- This can be accomplished by combining 3D model fields with specific observations related to the atmospheric forcings; when defining new observational programs more attention should be paid to the observation of atmospheric tendencies
- Ensembles should be used in case the available observations needed to constrain the wind field are insufficient or inadequate.

Future steps in setting up case studies of SBL processes were formulated in [Beljaars et al. \(2012\)](#). These may include the weak wind SBL where longwave radiation has a dominant role and where turbulence is intermittent. Another route is towards surface heterogeneity, which is expected to have important consequences for the behaviour of the SBL.

In the Appendix a full description of the data for the case is given. CESAR observations, which can be used for model evaluation of this case, can be downloaded from <http://www.knmi.nl/samenw/gabls>.

Acknowledgments The authors acknowledge Sander Tijn, Geert Lenderink, Henk Klein Baltink (all KNMI), Bas van de Wiel (Eindhoven University of Technology) and Sukanta Basu (North-Carolina State University) for fruitful discussions. G.J. Steeneveld acknowledges financial support from the BSIK-ME2 (Climate Changes Spatial Planning) research program.

Appendix: Case Set-Up

Here we describe in detail the preparation of a single column model run for the GABLS3 SCM case. Profiles and time series are given at the nodes (in height or time) of piecewise linear function. Modellers have to perform linear interpolation between these nodes where appropriate given their specific model grid and timesteps. When two node values at the same height or time are given, a jump (discontinuity) is implied. The first value should be prescribed up to the height or time specified. At the next model level or model timestep the second value should be prescribed.

Location

Cabauw, The Netherlands (51.9711°N, 4.9267°E, −0.7 m above sea level).

Period

1 July 2006 1200 to 2 July 2006 1200 UTC.

Surface and Soil Parameters

Surface parameters are listed in [Table 1](#). If a model discriminates between albedo for near infrared and visible light, the same values for both bands should be used. The band albedos are not known for Cabauw. If possible prescribe soil type as clay. Typical values for constituents are: 45 % clay, 8 % organic matter, no sand.

Table 1 Surface parameters for the Cabauw site

Name	Symbol	Value	Units
Albedo	a	0.23	–
Emissivity	ε	0.99	–
Roughness length for momentum	z_{0M}	0.15	m
Roughness length for heat	z_{0H}	0.0015	m
Vegetation fraction	f_{veg}	100	%
Leaf area index	LAI	2.0	–
Soil water content at field capacity	θ_{fc}	0.47	$m^3 m^{-3}$

Table 2 Initial soil temperature profile

Depth (m)	T_S (°C)
0.00	23.4
0.02	22.2
0.04	21.4
0.06	20.6
0.08	19.8
0.12	19.0
0.20	17.9
0.30	17.5
0.50	16.0
1.00	12.2
2.00	10.0
∞	10.0

Initial Conditions

Initial values are valid for 1 July 2006 1200 UTC, with a surface pressure of 1,024.4 hPa. The model soil water content is initialized such that the Bowen ratio is 0.33 at the start of the simulation. The initial soil temperature profile is given in Table 2. Models where the top soil layer is in direct contact with the atmosphere (no skin layer) do need some spin-up time. The initial atmospheric profiles of temperature and specific humidity are given in Table 3. Note that the value at zero height is a neutral extrapolation of the value at 2-m height. The model surface temperature will reach a model dependent value after the first timestep. The initial profile of wind is given in Table 4.

Atmospheric Forcings

Table 5 lists the geostrophic surface wind; at each timestep a vertical profile of geostrophic wind is obtained by linear interpolation between the prescribed surface geostrophic wind and $U_G = -2.0 m s^{-1}$ and $V_G = 2.0 m s^{-1}$ at 2,000 m. Above 2,000 m the geostrophic wind is constant.

Table 3 Initial profile of temperature and specific humidity. TOA is top of atmosphere

z (m)	T ($^{\circ}\text{C}$)	q (g kg^{-1})
0	27.0	9.3
2	27.0	9.3
10	26.4	8.5
20	26.2	8.4
40	25.9	8.3
80	25.5	8.2
140	24.8	8.1
205	24.3	8.0
1,800	9.0	7.5
2,200	09.0	2.0
5,000	-6.4	0.3
12,000	-61.0	0.01
14,000	-54.0	0.003
TOA	-50.0	0.000

Table 4 Horizontal wind, where U is the zonal wind component positive moving west to east, V is the meridional wind component positive moving south to north

z (m)	U (m s^{-1})	V (m s^{-1})
0	0.0	0.0
10	-4.0	-0.4
353	-5.5	-0.5
1,238	-5.5	-0.5
2,000	-2.0	2.0
TOA	-2.0	2.0

Table 5 Surface geostrophic wind

Time (UTC)	U_G (m s^{-1})	V_G (m s^{-1})
1 July 2006 1200	-7.8	0
1 July 2006 1800	-7.8	0
1 July 2006 2300	-6.5	4.5
2 July 2006 0300	-5.0	4.5
2 July 2006 0600	-5.0	4.5
2 July 2006 1200	-6.5	2.5

Table 6 Vertical movement in the layer between 1,500–5,000 m

Time (UTC)	ω (Pa s^{-1})
1 July 2006 1200	0.12
1 July 2006 1700	0.12
1 July 2006 1900	0.00
2 July 2006 1200	0.00

The vertical dynamical tendency is constant in the layer $z = 1,500\text{--}5,000$ m, and its change in time is given in Table 6. Above 5,000 m it is set to zero, and below 1,500 m it is interpolated linearly to zero at $z = 0$.

Table 7 Temperature dynamical tendency (200–1,000 m)

Time (UTC)	T_{adv} (K s ⁻¹)
1 July 2006 1200	-2.5×10^{-5}
2 July 2006 0100	-2.5×10^{-5}
2 July 2006 0100	7.5×10^{-5}
2 July 2006 0600	7.5×10^{-5}
2 July 2006 0600	0.0×10^{-5}
2 July 2006 1200	0.0×10^{-5}

Table 8 Specific humidity dynamical tendency (200–1,000 m)

Time (UTC)	q_{adv} (kg kg ⁻¹ s ⁻¹)
1 July 2006 1200	0
1 July 2006 2100	0
1 July 2006 2100	8.0×10^{-8}
2 July 2006 0000	8.0×10^{-8}
2 July 2006 0000	0
2 July 2006 0200	0
2 July 2006 0200	-8.0×10^{-8}
2 July 2006 0500	-8.0×10^{-8}
2 July 2006 0500	0
2 July 2006 1200	0

Table 9 Horizontal wind dynamical tendency (200–1,000 m)

Time (UTC)	U_{adv} (m s ⁻²)	V_{adv} (m s ⁻²)
1 July 2006 1200	0	0
1 July 2006 1800	0	0
1 July 2006 1800	-1.5×10^{-4}	1.0×10^{-4}
1 July 2006 2300	-1.5×10^{-4}	1.0×10^{-4}
1 July 2006 2300	5.0×10^{-4}	0.0×10^{-4}
2 July 2006 0300	5.0×10^{-4}	0.0×10^{-4}
2 July 2006 0300	0	0
2 July 2006 1200	0	0

All the horizontal dynamical tendencies are prescribed constant in the layer $z = 200$ – $1,000$ m. They are listed in Tables 7, 8 and 9 for temperature, specific humidity and wind respectively. Above $z = 1,500$ m and at $z = 0$ all advective terms are zero. Above $1,000$ m we apply a linear interpolation to zero at $1,500$ m; below 200 m apply a linear interpolation to zero at $z = 0$.

References

Baas P (2009) Turbulence and low-level jets in the stable boundary layer. Thesis, Wageningen University, Wageningen, NL. ISBN 978-90-8585-446-3, 152 pp

- Baas P, Bosveld FC, Klein Baltink H, Holtslag AAM (2009) A climatology of nocturnal low-level jets at Cabauw. *J Appl Meteorol Climatol* 48:1627–1642
- Baas P, Bosveld FC, Lenderink G, van Meijgaard E, Holtslag AAM (2010) How to design single-column model experiments for comparison with observed nocturnal low-level jets? *Q J R Meteorol Soc* 136:671–684
- Basu S, Holtslag AAM, van de Wiel BJH, Moene AF, Steeneveld G-J (2008) An inconvenient “truth” about using sensible heat flux as a surface boundary condition in models under stably stratified regimes. *Acta Geophys* 56:88–99
- Basu S, Holtslag AAM, Bosveld FC (2012) GABLS3 LES intercomparison study. In: ECMWF/GABLS workshop on “Diurnal cycles and the stable atmospheric boundary layer. ECMWF, pp 75–82. www.ecmwf.int
- Beare RJ, MacVean MK, Holtslag AAM, Cuxart J, Esau I, Golaz J-C, Jimenez MA, Khairoutdinov M, Kosovic B, Lewellen D, Lund TS, Lundquist JK, McCabe A, Moene AF, Noh Y, Raasch S, Sullivan PP (2006) An intercomparison of large-eddy simulations of the stable boundary layer. *Boundary-Layer Meteorol* 118:247–272
- Beljaars ACM (1987) On the memory of wind standard deviation for upstream roughness. *Boundary-Layer Meteorol* 38:95–101
- Beljaars ACM, Bosveld FC (1997) Cabauw data for the validation of land surface parameterization schemes. *J Clim* 10:1172–1193
- Beljaars ACM, Viterbo P (1998) Role of the boundary layer in a numerical weather prediction model. In: Holtslag AAM, Duynkerke PG (eds) Clear and cloudy boundary layers. Royal Netherlands Academy of Arts and Sciences, North Holland Publishing Company, Amsterdam, p 372
- Beljaars ACM, Svensson G, Holtslag AAM (2012) Working group reports. In: The proceedings of the ECMWF workshop on diurnal cycles and the stable boundary layer, 7–10 November 2011, Reading, UK
- Bergamaschi P, Krol M, Meirink JF, Dentener F, Segers A, van Aardenne J, Monni S, Vermeulen AT, Schmidt M, Ramonet M, Yver C, Meinhardt F, Nisbet EG, Fisher RE, O’Doherty S, Dlugokencky EJ (2010) Inverse modeling of European CH₄ emissions 2001–2006. *J Geophys Res* 115:D22309
- Bergot T, Terradellas E, Cuxart J, Mira A, Liechti O, Mueller M, Nielsen NW (2007) Intercomparison of single-column numerical models for the prediction of radiation fog. *J Appl Meteorol Climatol* 46:504–521
- Bosveld FC, van Meijgaard E, Moors E, Werner C, (2004) Interpretation of eddy-correlation flux observations at different levels along the Cabauw 200 m meteorological mast. Extended abstract. In: 16th AMS symposium on boundary layer and turbulence, 9–13 August 2004, Portland, ME, USA, American Meteorological Society, Boston
- Bosveld FC, Baas P, Steeneveld G-J, Holtslag AAM, Angevine WM, Bazile E, de Bruijn EIF, Deacu D, Edwards JM, Ek M, Larson VE, Malardel S, Pleim JE, Raschendorfer M, Svensson G (2014) The third GABLS intercomparison case for boundary layer model evaluation. Part B: Results and process understanding. *Boundary-Layer Meteorol*. doi:10.1007/s10546-014-9919-1
- Brutsaert WH (1982) Evaporation into the atmosphere. D. Reidel Publishing Company, Dordrecht 299 pp
- Casso-Torralba P, Vilà-Guerau de Arellano J, Bosveld FC, Soler MR, Vermeulen A, Werner C, Moors E (2008) Diurnal and vertical variability of the sensible heat and carbon dioxide budgets in the atmospheric surface layer. *J Geophys Res* 113:D12119
- Cuxart J, Holtslag AAM, Beare RJ, Bazile E, Beljaars ACM, Cheng A, Conangla L, Ek MB, Freedman F, Hamdi R, Kerstein A, Kitagawa H, Lenderink G, Lewellen D, Mailhot J, Mauritsen T, Perov V, Schayes G, Steeneveld G-J, Svensson G, Taylor P, Weng W, Wunsch S, Xu KM (2006) Single-column model intercomparison for a stably stratified atmospheric boundary layer. *Boundary-Layer Meteorol* 118:273–303
- Edwards JM, Beare RJ, Lapworth AJ (2006) Simulation of the observed evening transition and nocturnal boundary layers: single-column modelling. *Q J R Meteorol Soc* 132:61–80
- Holtslag AAM (2003) GABLS initiates intercomparison for stable boundary layers. *GEWEX News* 13:7–8
- Holtslag AAM (2006) Preface: GEWEX Atmospheric Boundary-layer Study (GABLS) on stable boundary layers. *Boundary-Layer Meteorol* 118:243–246
- Holtslag AAM, Steeneveld G-J, van de Wiel BJH (2007) Role of land-surface temperature feedback on model performance for the stable boundary layer. *Boundary-Layer Meteorol* 125:361–376
- Holtslag AAM, Svensson G, Baas P, Basu S, Beare B, Beljaars ACM, Bosveld FC, Cuxart J, Steeneveld GJ, Tjernström M, van de Wiel BJH (2013) Stable atmospheric boundary layers and diurnal cycles—challenges for weather and climate models. *Bull Am Meteorol Soc* 94:1691–1706
- Jung T, Balsamo G, Bechtold P, Beljaars ACM, Köhler M, Miller MJ, Morcrette J-J, Orr A, Rodwell MJ, Tompkins AM (2010) The ECMWF model climate: recent progress through improved physical parameterizations. *Q J R Meteorol Soc* 136:1145–1160
- King JC, Connolley WM, Derbyshire SH (2001) Sensitivity of modelled Arctic climate to surface and boundary-layer parameterizations. *Q J R Meteorol Soc* 127:779–794

- King JC, Jrrar A, Connolley WM (2007) Sensitivity of modelled atmospheric circulation to the representation of stable boundary layer processes. *Geophys Res Lett* 34:L06708
- Lauvaux T, Gioli B, Sarrat C, Rayner PJ, Ciais P, Chevallier F, Noilhan J, Miglietta F, Brunet Y, Ceschia E, Dolman H, Elbers JA, Gerbig C, Hutjes R, Jarosz N, Legain D, Uliasz M (2009) Bridging the gap between atmospheric concentrations and local ecosystem measurements. *Geophys Res Lett* 36:L19809
- Lenderink G, Siebesma AP, Chenet S, Ihrns S, Jones CG, Marquet P, Muller F, Olmeria D, Calvo J, Sanchez E, Soares PMM (2004) The diurnal cycle of shallow cumulus clouds over land: a single-column model intercomparison study. *Q J R Meteorol Soc* 130:3339–3364
- Negggers RAJ, Siebesma AP, Heus AT (2012) Continuous single-column model evaluation at a permanent meteorological supersite. *Bull Am Meteorol Soc* 93(9):1389–1400
- Nieuwstadt FTM, Driedonks AGM (1979) The nocturnal boundary layer: a case study compared with model calculations. *J Appl Meteorol* 18:1397–1405
- Poulos GS, Coauthors (2002) CASES-99: a comprehensive investigation of the stable nocturnal boundary layer. *Bull Am Meteorol Soc* 83:555–581
- Prabha TV, Hoogenboom G, Smirnova TG (2011) Role of land surface parameterizations on modelling cold-pooling events and low-level jets. *Atmos Res* 99:147–161
- Russchenberg H, Bosveld FC, Swart D, ten Brink H, de Leeuw G, Uijlenhout R, Abresser-Rastburg B, van der Marel H, Ligthart L, Boers R, Apituley A (2005) Ground based atmospheric remote sensing in the Netherlands: European outlook. *IEICE Trans Commun* E88–B(6):2252–2258
- Salmond JA, McKendry IG (2005) A review of turbulence in the very stable nocturnal boundary layer and its implications for air quality. *Prog Phys Geogr* 29:171–188
- Siebesma AP, Jakob C, Lenderink G, Neggers RAJ, Teixeira J, van Meijgaard E, Calvo J, Chlond A, Grenier H, Jones C, Kohler M, Kitagawa H, Marquet P, Lock AP, Muller F (2004) Cloud representation in general circulation models over the Northern Pacific Ocean: a EUROCS intercomparison study. *Q J R Meteorol Soc* 130:3245–3267
- Skamarock WC, Klemp JB (2008) A time-split nonhydrostatic atmospheric model for weather research and forecasting applications. *J Comput Phys* 227(7):3465–3485
- Steenefeld G-J, van de Wiel BJH, Holtslag AAM (2006) Modeling the evolution of the atmospheric boundary layer coupled to the land surface for three contrasting nights in CASES-99. *J Atmos Sci* 63:920–935
- Storm BJ, Dudhia J, Basu S, Swift A, Giammanco I (2009) Evaluation of the weather research and forecasting model on forecasting low-level jets: implications for wind energy. *Wind Energy* 12:81–90
- Svensson G, Holtslag AAM (2009) Analysis of model results for the turning of the wind and related momentum fluxes in the stable boundary layer. *Boundary-Layer Meteorol* 132:261–277
- Svensson G, Holtslag AAM, Kumar V, Mauritsen T, Steeneveld GJ, Angevine WM, Bazile E, Beljaars A, de Bruijn EIF, Cheng A, Conangla L, Cuxart J, Ek M, Falk MJ, Freedman Kitagawa H, Larson VE, Lock A, Mailhot J, Masson V, Park S, Pleim J, Söderberg S, Zampieri M, Weng W (2011) Evaluation of the diurnal cycle in the atmospheric boundary layer over land as represented by a variety of single-column models - the second GABLS experiment. *Boundary-Layer Meteorol* 140:177–206
- Teixeira J, Miranda PMA (2001) Fog prediction at Lisbon airport using a one-dimensional boundary layer model. *Meteorol Appl* 8:497–505
- Tijm ABC, van Delden AJ, Holtslag AAM (1999) The inland penetration of sea breeze. *Contr Atmos Phys* 72:317–328
- Tolk LF, Peters W, Meesters AGCA, Groenendijk M, Vermeulen AT, Steeneveld GJ, Dolman AJ (2009) Modelling regional scale surface fluxes, meteorology and CO₂ mixing ratios for the Cabauw tower in the Netherlands. *Biogeoscience* 6:2265–2280
- Undén P et al (2002) HIRLAM-5 scientific documentation. HIRLAM-5 Project, SMHI, Norrköping, Sweden, 146 pp
- van Delden AJ (1993) Observational evidence of the wave-like character of the sea breeze effect. *Beitr Phys Atmos* 66:63–72
- van de Wiel BJH, Moene AF, Hartogensis OK, de Bruin HAR, Holtslag AAM (2003) Intermittent turbulence in the stable boundary layer over land. Part III: a classification for observations during CASES-99. *J Atmos Sci* 60:2509–2522
- van der Velde IR, Steeneveld GJ, Wichers Schreur BGJ, Holtslag AAM (2010) Modeling and forecasting the onset and duration of severe radiation fog under frost conditions. *Mon Weather Rev* 138:4237–4253
- Van Heerwaarden CC, Vila-Guerau de Arellano J, Moene AF, Holtslag AAM (2009) Interactions between dry-air entrainment, surface evaporation and convective boundary layer development. *Q J R Meteorol Soc* 135:1277–1291
- van Meijgaard E, van Ulft LH, van de Berg WJ, Bosveld FC, van den Hurk BJJM, Lenderink G, Siebesma AP (2008) The KNMI regional atmospheric climate model RACMO, version 2.1. KNMI publication: TR-302, 24/12/2008, De Bilt, The Netherlands, 43 pp

- van Ulden AP, Wieringa J (1996) Atmospheric boundary layer research at Cabauw. *Boundary-Layer Meteorol* 78:39–69
- Verkaik JW, Holtslag AAM (2007) Wind profiles, momentum fluxes and roughness lengths at Cabauw revisited. *Boundary-Layer Meteorol* 122:701–719
- Walsh JE, Chapman WL, Romanovsky V, Christensen JH, Stendel M (2008) Global climate model performance over Alaska and Greenland. *J Clim* 21:6156–6174
- Wong KW, Stutz J (2010) Influence of nocturnal vertical stability on daytime chemistry: a one-dimensional model study. *Atmos Environ* 44:3753–3760